Orientational ordering of point dipoles on a sphere

Andraž Gnidovec ⬤ and Simon Čopar

Faculty of Mathematics and Physics, University of Ljubljana, SI-1000 Ljubljana, Slovenia

Arrangement of interacting particles on a sphere is historically a well-known problem, however, ordering of particles with anisotropic interaction, such as the dipole-dipole interaction, has remained unexplored. We calculate the equilibrium orientational ordering of point dipoles on a sphere with fixed positional order with numerical minimization of interaction energy and analyze stable configurations depending on their symmetries and degrees of ordering. We find that a macrovortex is a generic ground state for locally triangular spherical lattices with various discrete rotational symmetries for different system sizes, whereas higher-energy metastable states are similar but less ordered. We observe orientational phase transitions and hysteresis in response to changing external field both for the fixed sphere orientation with respect to the field as well as for a freely rotating sphere. For the case of a freely rotating sphere, we also observe changes in the symmetry axis with increasing field strength.

I. INTRODUCTION

The nature of minimal energy distributions of interacting particles on a sphere is a well-known question both for its historical significance and for its contemporary relevance. Since Thomson proposed his model of an atom in 1897 and, in turn, sought configurations with minimal energy for N same-charged particles on the surface of a sphere [1], the problem has been generalized to different interparticle interactions, most notably, different long-range power-law [2] and logarithmic [3] interactions, Tammes problem of the packing of hard circles [4], and arrangement of connected charges [5]. Active research on different interaction potentials and geometric aspects of solutions continues to this day [6–10]. Investigation of sphere-bound particles under effect of generalized interactions gives insights into the symmetry and geometry of the resulting organizational order and yields descriptive models for various types of self-organized matter, such as arrangement of proteins in capsids [11,12], fullerene patterns in carbon clusters [13], and distribution of solid particles in Pickering emulsions [14].

In contrast with the body of research on isotropic particles, ordering of discrete particles with orientation-dependent interactions on a sphere has remained relatively unexplored. Anisotropy can be a consequence of noncircular hard particles [15], directed motion in dynamical systems [16–20], short-range nearest-neighbor couplings, such as approximate models of spin lattices, or, in general, induced by anisotropic long-range interactions. A natural anisotropic extension of the Thomson problem, which has not been considered before, is to extend the multipolar expansion to the dipolar term so that in addition to position, orientation of the polarization vector can be varied for each particle. Assuming the repulsive isotropic interactions between the particles are strong enough, a restricted problem can be considered, fixing the particle positions, and solving for polarization orientations that minimize

the electrostatic energy of the system. This is often the case for systems of hard particles and closely packed assemblies where anisotropic long-range interaction is a small perturbation on top of a sterically imposed positional lattice.

Spherical topology requires presence of defects that depend on the symmetry of local order. In the continuous limit, vectorial order on a sphere is topologically required by the hairy ball theorem to have, at least, two vortices [21], which are affected by the local Gaussian curvature [22]. Continuous counterparts of a system of discrete dipoles on a sphere, such as ferromagnetic spherical shells [23] and Heisenberg spin systems [24], show different magnetization states, including a state with polar vortices. On a discrete spherical lattice, both the local geometry of the lattice and topology of the sphere affect the ground-state structure. Although the topology prevents us from fitting any regular lattice onto its surface [25], planar solutions can shed light on local behavior of dipole systems on a sphere and help with interpretations of the results. Two-dimensional (2D) dipolar systems appear in many fields from magnetic beads sold as novelty toys to electrostatic interactions of colloidal nanoparticles [26,27] and magnetic nanostructures [28]. Theoretical analysis of energy ground states of 2D dipolar lattices have been copiously studied during the previous century, showing antiferromagnetic states, periodic vortex states, and macrovortex states, depending on the positional lattice [29–31]. It was found that, considering the long-range nature of dipole-dipole interactions, instead of using a nearest-neighbor approximation, has a determining effect on orientational ordering and structural phase transitions [32]. Planar and spherical geometry are a starting point to general three-dimensional (3D) self-assembly that can be guided by anisotropic interactions, such as patchy-particle or dipolar interactions, and can contribute to creation of new functional materials and metamaterials [33,34].

In this paper, we investigate ground-state orientations of point dipoles on a sphere, positionally fixed to a uniform

spherical lattice, and study the effects of local positional order on dipolar structures. The paper is organized as follows. We start by defining the energy functional, describe the simulation methods used to find the ground states of dipolar systems on a sphere, and introduce order parameters for quantitative analysis of order. We present the results of numerical simulations and show that for uniform spherical lattices, the ground states have a macrovortex structure for all numbers of dipoles if local positional order resembles that of the triangular lattice. Oblique angles in the lattice can disrupt the macrovortex state. We further study the effects of external field on dipole configurations and the resulting orientational phase transitions both for fixed field direction and for the case of a freely rotating sphere. In the latter case, different system configurations merge as the field magnitude increases, and for certain states, we also observe the change in configuration symmetry.

II. SIMULATION METHODS

We consider a system of N dipoles $\{\boldsymbol{p}_i\}$ fixed at points in space $\{\boldsymbol{r}_i\}$ and in the presence of an external field $\boldsymbol{H}$. Such as in the standard Thomson problem, interactions between all particle pairs are taken into account. The nondimensional energy of our system, appropriate to model either electrostatic or magnetic dipoles, is

$$\mathcal{U} = \sum_{\substack{i,j=1 \\ i \neq j}}^{N} \frac{\boldsymbol{p}_i \cdot \boldsymbol{p}_j - 3(\boldsymbol{p}_i \cdot \hat{\boldsymbol{r}}_{ij})(\boldsymbol{p}_j \cdot \hat{\boldsymbol{r}}_{ij})}{r_{ij}^3} - \boldsymbol{H} \cdot \sum_{i=1}^{N} \boldsymbol{p}_i, \quad (1)$$

where the first term represents dipole-dipole contribution and the second term describes interaction of dipoles with the external field. We denoted $\boldsymbol{r}_{ij} = \boldsymbol{r}_j - \boldsymbol{r}_i$ and hat over a vector represents a unit vector in the same direction. The positional order is determined by one of the uniform point distributions on a sphere; we consider solutions of the Thomson and Tammes problems as well as the Fibonacci spherical distribution. Orientations of dipoles are parametrized by two angles, azimuthal angle ϕ_i and polar angle θ_i in their respective local coordinate frames. We solve the problem of energy minimization numerically. We explore systems of size $N < 200$ and chose Broyden-Fletcher-Goldfarb-Shanno minimization algorithm as both an effective and time-efficient method to find ground states and other stable configurations in zero external field. The results of the minimization can depend on the initial configuration—the minimization algorithm can get trapped in a metastable configuration, resulting in a large number of states with different degrees of ordering. We perform the minimization repeatedly from random initial conditions to ensure finding the global minimum. As the number of metastable states grows exponentially with the system size, values of N much higher than the selected limit $N = 200$ are computationally not worth pursuing in this manner. Stohastic methods should be used instead and have in the past proven useful in analyzing different multipolar systems [35–37]. Nevertheless, we argue in the following section that ground-state structures in systems with high N are qualitatively the same as for the smaller systems. With much larger N, a continuum limit is approached, lattice defects become less and less important,
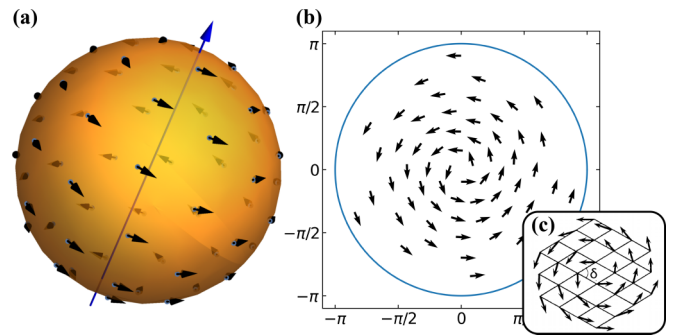

FIG. 1. (a) Three-dimensional (3D) visualization of the ground-state configuration for $N = 60$. Macrovortex orientation is formed where the orientation of dipole moments is characterized by the direction of angular momentum $\boldsymbol{\Gamma}$, here, represented by the blue arrow. (b) The same configuration showed in azimuthal projection. The direction of $\boldsymbol{\Gamma}$ defines the north pole of the sphere and lies in the center of the diagram. The entire blue circle represents the south pole. (c) The ground state of a dipolar system on the hexagonal lattice is also a macrovortex (adapted from Ref. [31]).

and the surface of the sphere locally resembles a 2D Euclidean lattice, which has been studied before [31].

To quantitatively measure the order and compare various configurations, we need suitable order parameters. The choice of parameters depends on expected ordering of dipoles. Consider results of the energy minimization for 2D lattice dipolar systems. For square and hexagonal lattices, the ground state is infinitely degenerate and periodic [29]. For rhombic lattices with angles of rhombicity between $\delta = 50°$ and $\delta = 75°$, which include the special case of the triangular lattice at $\delta = 60°$, the ground state is found to be a macrovortex [31,32,38]. Both the Thomson and Tammes lattices locally resemble the triangular lattice; with the exception of lattice defects, topologically required by the Euler characteristic of the sphere, most vertices have six nearest neighbors. In contrast, the Fibonacci lattice shows a different local positional order which also affects dipolar configurations. We discuss this more thoroughly in the following section.

Our calculations confirm that the macrovortex structure is also the ground state of the dipolar system on a sphere with positional order fixed to the Thomson or Tammes positions. Figure 1(a) shows the ground-state configuration for the $N = 60$ Thomson lattice. The macrovortex structure stands out even more in the azimuthal projection in Fig. 1(b), shown in comparison to the macrovortex on the 2D triangular lattice [Fig. 1(c)]. The behavior of 2D lattice dipolar systems in an external field also gives an indication of the expected field response for dipolar systems on a sphere. For example, a hexagonal lattice was shown to have a discontinuous orientational phase transition in the external field [30], leading us to expect similar behavior for spherical dipolar systems.

To determine the axis of rotation and quantify the macrovortex nature of the ground states, we define the angular momentum,

$$\boldsymbol{\Gamma} = \frac{1}{N} \sum_{i=1}^{N} \hat{\boldsymbol{r}}_i \times \hat{\boldsymbol{p}}_i. \quad (2)$$

The magnitude Γ gives us information on the intensity of this circulation and can be related to the coefficient of the curl term $\boldsymbol{\Psi}_{lm} = \boldsymbol{r} \times \nabla Y_{\ell m}$ of vector spherical harmonics expansion [39] at $\ell = 1$. For analysis of more complicated states where higher-order variations and radial and gradient components are also significant, a complete expansion of dipole orientations over vector spherical harmonics would provide additional insight.

To explore the response of the system to external magnetic-field $\boldsymbol{H}$, we further define magnetization,

$$\boldsymbol{M} = \frac{1}{N} \sum_{i=1}^{N} \boldsymbol{p}_i, \qquad (3)$$

and susceptibility,

$$\chi = \frac{dM_\parallel}{dH}, \qquad (4)$$

where $M_\parallel$ denotes the component of magnetization in the direction of $\boldsymbol{H}$. For calculations of response to the external field where the system must stay in the same local minimum during changes in the field and starting from the chosen stable configuration, we use a simple relaxation method (gradient descent). Our energy functional (1) is a quadratic form and relaxation, therefore, reduces to iterative application of a linear transformation and renormalization of dipole moments. As we gradually increase the magnitude of the external field, we calculate magnetization and susceptibility at each step. This continuity of states is also important in measuring the hysteresis response.

III. RESULTS

In this section, we present our simulation results, first focusing on analyzing different stable states found on the Thomson lattice and comment on the role of local positional order on ground-state configurations. Further results on the Tammes and Fibonacci lattices can be found in the Supplemental Material (SM) [40]. We also explore the effects of an external magnetic field on stable states both for the fixed direction of the field as well as for the case of a freely rotating sphere.

A. Stable configurations

We performed 1000 minimization simulations at each N for different spherical lattices to examine the dependence of ground-state energy and the number of all states found on the number of dipoles and positional order (Fig. 2). In all obtained configurations, we observe that, in the absence of an external field, dipoles orient tangentially to the surface of the sphere. This is in line with expectations considering the locally preferred configuration of neighboring dipoles is head to tail and taking into account that in the true ground-state configuration of a long-range interacting dipole system, dipoles orient in a way that minimizes bulk magnetization $\boldsymbol{M}$ [31]. To improve time efficiency of the simulation, one can, therefore, constrain dipole orientations to their respective tangent planes, which reduces the dimension of the minimization from $2N$ to N and yields $\approx 4 \times$ improvement in calculation times. These ground states can, then, be further minimized over full set
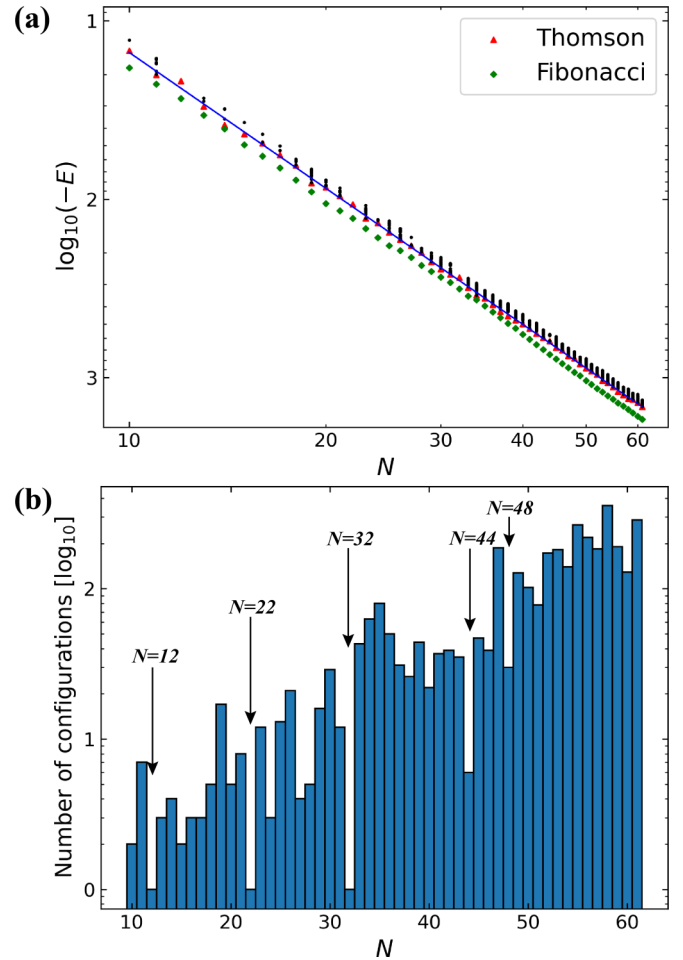

FIG. 2. Results of 1000 randomly initialized minimizations for all N between 10 and 61. (a) Energies of all found dipole configurations on the Thomson lattice (ground-state energies are represented by red marks whereas excited-state energies are shown in black) along with ground-state energies on the Fibonacci lattice (green marks). We also fit a power law to Thomson ground-state energies and determine scaling as $E_0 \sim N^{2.495}$. (b) Number of different configurations found for each N shows exponential growth trend (note the logarithmic scale on the y axis). Arrows indicate N that correspond to symmetric lattices, which have a much smaller number of local minima.

of orientational degrees of freedom without the tangential constraint without much additional computational effort. We used general 3D minimization for $N \leqslant 100$ where we were also interested in the number of stable configurations and 2D minimization with subsequent 3D relaxation for $N > 100$.

We find that the ground-state energy decreases monotonously for all three lattices and can be fitted by power-law curves $E_0 \propto N^{2.495}$, $E_0 \propto N^{2.508}$, and $E_0 \propto N^{2.504}$ for the Thomson, Tammes, and Fibonacci lattice, respectively. These exponent values are close to the estimate $5/2$ we get by taking into account scaling of the distance between dipoles as $r \propto N^{-1/2}$ and energy as $E \propto N/r^3$. Figure 2(a) shows that dipolar ground-state energies for the Fibonacci lattice are consistently lower that those on the equivalently sized Thomson lattice as well as the Tammes lattice due to shortest

distances between neighbors being larger in the more uniform Thomson and Tammes lattices. The latter are not shown in the plot as they are very close to the Thomson ground-state energies.

The dependence of the number of different configurations (local minima) on N is more complicated and strongly connected to the symmetry of positional order as is shown in Fig. 2(b) for the Thomson lattice. We note the trend of exponential increase of found local minima with N, which is expected as higher number of dipoles on the sphere allows for a larger number of stable yet frustrated local configurations that prevent global ordering. Systems with low numbers of found states can be linked to highly symmetric lattices. The cases that stand out the most are $N = 12$, $N = 22$, and $N = 32$ with only one configuration and $N = 44$ with six configurations, with icosahedral, tetrahedral, icosahedral, and octahedral positional order symmetries, respectively. The number of found states on the Tammes and Fibonacci lattices further confirms the dependence on the discrete rotational lattice symmetries. Numbers of states on the Fibonacci lattice, which lacks any symmetries, only show exponential growth whereas Tammes lattices show expected dips at more symmetric configurations (see the SM [40]).

We now examine individual cases of stable structures, focusing primarily on the solutions for the Thomson lattice as they enable us to study the role of lattice symmetry on dipolar configuration. Later, we also comment on solutions with Tammes and Fibonacci positional order. First, we look at the ground state for $N = 12$ [Fig. 3(a)]. A macrovortex configuration is formed which reduces the symmetry of the solution from icosahedral symmetry of the positional order to the point group C_3. The direction of angular momentum $\mathbf{\Gamma}$ corresponds to the threefold rotation axis of the configuration. All of the dipoles lie on four planes perpendicular to $\mathbf{\Gamma}$ with their dipole moments also parallel to these planes. The magnitude of angular momentum is $\Gamma = 0.795$ which is close to the analytical estimate of $\pi/4 \approx 0.785$ for continuous distribution of dipoles arranged in a macrovortex (the deviation, here, is the consequence of discretization). Also possible are configurations with a fourfold symmetry axis, for instance, the ground state for $N = 24$ shown in Fig. 3(b). The magnitude of $\mathbf{\Gamma}$ is again close to the analytical estimate, a characteristic that also holds for macrovortex states at other N's and can, therefore, be used as an indicator for the degree of ordering with less ordered configurations described by a lower value of Γ.

We further look at four different configurations of $N = 72$ dipoles where positional order again has icosahedral symmetry [Fig. 3(c)]. The number of different states found in 1000 minimization simulations is 41, low for a system of this size, which is expected. We use azimuthal projection for better visualization. The ground state (top left panel) and first excited state (top right panel) show the formation of two distinct macrovortex structures with the first being less symmetric (twofold symmetry) than the second (threefold symmetry). As an illustration of possible partially ordered and disordered states that emerge for higher numbers of dipoles, we also show configurations for the fifth (bottom left panel) and thirty-third (bottom right panel) excited states. The magnitude of angular momentum decreases as the macrovortex ordering disappears.
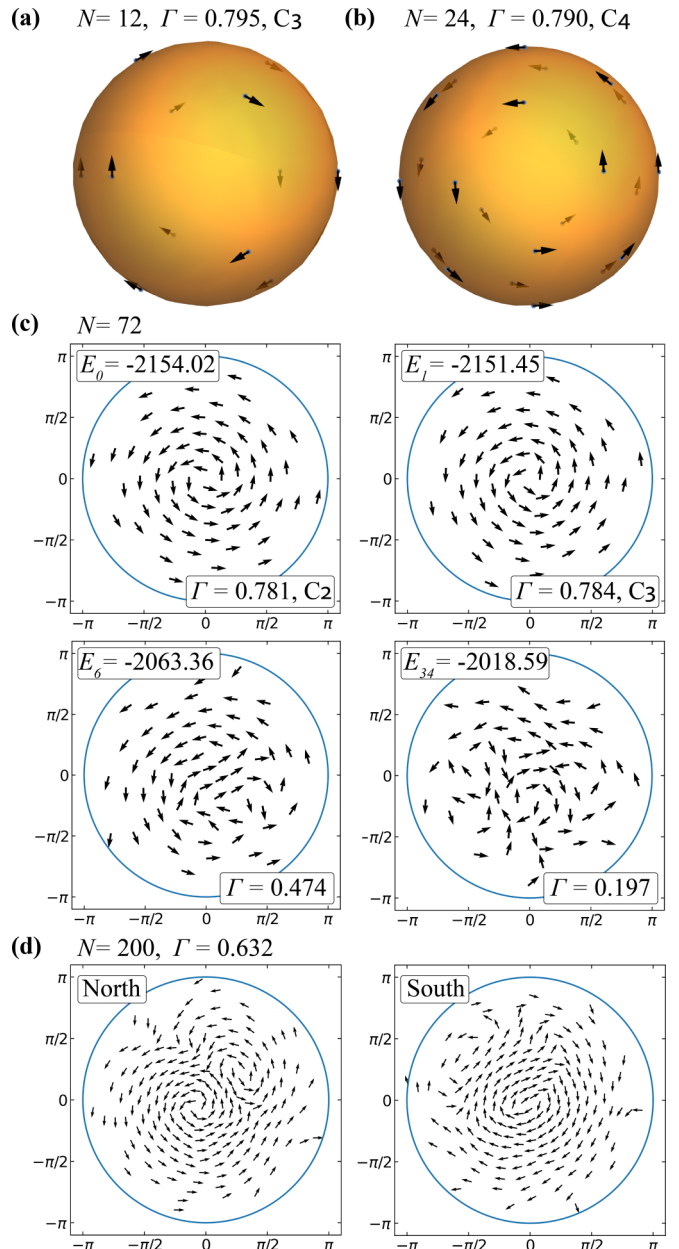

FIG. 3. Visualization of some configurations at selected N. Angular momentum magnitude characterizes the degree of order in the system with values close to $\pi/4 \approx 0.785$ indicating a macrovortex structure and lower values related to less ordered configurations. (a) Ground-state configuration for $N = 12$ shows C_3 symmetry. All dipoles are also aligned on planes perpendicular to the direction of $\mathbf{\Gamma}$. (b) Ground-state configuration for $N = 24$ belongs to the C_4 point group. (c) Azimuthal projections for the ground state and three excited states of the $N = 72$ case. The first two states show different macrovortex configurations—the ground-state configuration has a twofold symmetry axis whereas the first excited state has a threefold axis. We also show one of the partially ordered states where only approximately half of all dipoles are oriented in a vortex whereas the rest are disordered and one of disordered states. (d) One of the possible excited states for $N = 200$. Two competing vortices of the same orientation are formed which leads to antiparallel orientation of dipoles between the vortex sources and a single elongated vortex on the south pole of the sphere (left panel).

In the first case, approximately one half of dipoles is already forming a macrovortex, however, the other dipoles are locked in a different configuration (local energy minimum). Similarly, the last case shows the formation of dipole strings (head-to-tail configurations of neighbor dipoles) that are also metastable.

If we increase the number of dipoles N even further, another possible excited-state configuration emerges. Instead of a single macrovortex, two competing vortices lying side by side and oriented in the same direction are formed [Fig. 3(d)]. This results in an antiparallel configuration of dipoles between the two vortex sources but preserves macrovortexlike orientational order at greater distances from both vortices so that, at the south pole, we only find one elongated vortex. Also possible are excited states with different arrangements and higher numbers of vortex domains.

In general, we find macrovortex ground states on the Thomson lattice for all values of N. This can also be confirmed by the values of Γ that are close to the analytical estimate of $\pi/4$ whereas lower values indicate less ordered configurations. An important question that arises is the effect of lattice defects for higher values of N in the form of topological scars on macrovortex dipolar ordering. We first note that centers of macrovortices are not directly correlated with the locations of lattice defects and are rather located at the edges or faces of the lattice triangulation. In many cases, these macrovortex centers correspond to lattice symmetry axes as seen in Figs. 3(a)–3(c), however, this does not hold, in general. Naturally, this cannot manifest in systems with no positional order symmetry but is also not true for some cases of highly symmetric lattices, e.g., $N = 32$. Consequently, positional order symmetry alone does not guarantee symmetrical configurations of dipolar ground states.

We further examine the role of local positional order on dipolar ordering in the SM [40] by looking at the ground-state structures on the Tammes and Fibonacci lattices. Similar to the Thomson lattice, the Tammes lattice is locally triangular, and we obtain virtually indistinguishable behavior of dipolar ordering. Macrovortex is the ground state for all N, independent of the lattice symmetry and defect structure. This shows that the macrovortex dipole structure emerges on all lattices that locally approximate an equilateral triangular lattice. It is stable to local imperfections of positional order in the form of scars and dislocations but can change significantly once the lattice deviates systematically from local triangular order. In the studied case of the Fibonacci lattice where points form a spiral from one pole to another, around the equator, the lattice locally resembles the square lattice (for high enough N) which leads to the formation of mutually parallel and antiparallel dipole strings (see the SM [40]). At the poles, which are privileged points on this lattice, the dipole strings follow the nearest neighbors. This behavior is consistent with the dependence of the ground state on the rhombic angle on planar lattices [31].

B. Fixed direction of the external field

The simulations for determining the response of stable dipole configurations on a sphere in the external field were performed using the relaxation approach that also models the correct system transitions under slow changes of external field. We show the results for the Thomson positional order that are relevant for all locally triangular lattices. The choice of the field direction has an important impact on the results. First, we restrict the field to point in the direction of angular momentum Γ of the ground state before application of the field, which represents the characteristic direction of dipolar order for each configuration (Fig. 4). Although this makes the comparison of behavior between different configurations difficult, it enables us to roughly grasp the properties of the system in an external field.

We start by examining the response for the simplest case of $N = 12$ [Fig. 4(a)]. Magnetization increases continuously until saturation and similarly, angular momentum magnitude drops to zero. This signals that the system undergoes a second-order orientational phase transition from the macrovortex to the total alignment with the field. The change in dipole directions can be seen in simulation frames taken at different external field magnitudes.

Continuous orientational phase transition is not a general result and emerges for $N = 12$ because of the positional order and configuration symmetry. We observe similar behavior for other configurations with C_n symmetry whereas ground states and excited states that are not symmetric exhibit different characteristics. Figure 4(b) shows the dependence of magnetization, susceptibility, and magnitude of angular momentum on the magnitude of the external field for three metastable configurations for $N = 13$. The ground state is a macrovortex whereas the excited states show nonregular ordering. All magnetization curves have, at least, one discontinuous jump that reflects in the divergence in susceptibility, signaling orientational phase transitions. To better understand the nature of these transitions, we look at the graphs of angular momentum magnitude where a general decrease in Γ shows that the dipoles are aligning with the field. More interesting is the discontinuous jump in Γ at the first phase transition where the system relaxes to a more ordered quasimacrovortex structure. To better imagine how the order of the system changes with the increasing magnetic field, we use azimuthal projection to show dipole orientations at different field magnitudes. The results for the first excited state of $N = 13$ are presented in Fig. 4(c). After the first orientational phase transition (frame 2), angular momentum shifts away from the direction of the field to form a new macrovortex configuration. After the second phase transition (frame 3), the dipoles order to form a dipole string, and, after the third transition, dipoles align with the external magnetic field. In the last frame, the direction of Γ is not shown anymore as its magnitude is too small for its direction to be relevant.

As an example of higher N, we show the magnetization and angular momentum magnitude graphs for the ground state and next three excited states of $N = 56$. The results are similar to ones for $N = 13$ with the second and fourth excited states undergoing more orientational phase transitions than the ground state. The configuration of the third excited state is also a macrovortex, and the number of discontinuous transitions is, therefore, lower.

At the end of this section, we look at the magnetization hysteresis loops obtained by decreasing the field magnitude after the system reaches saturation. The results for $N = 12$,
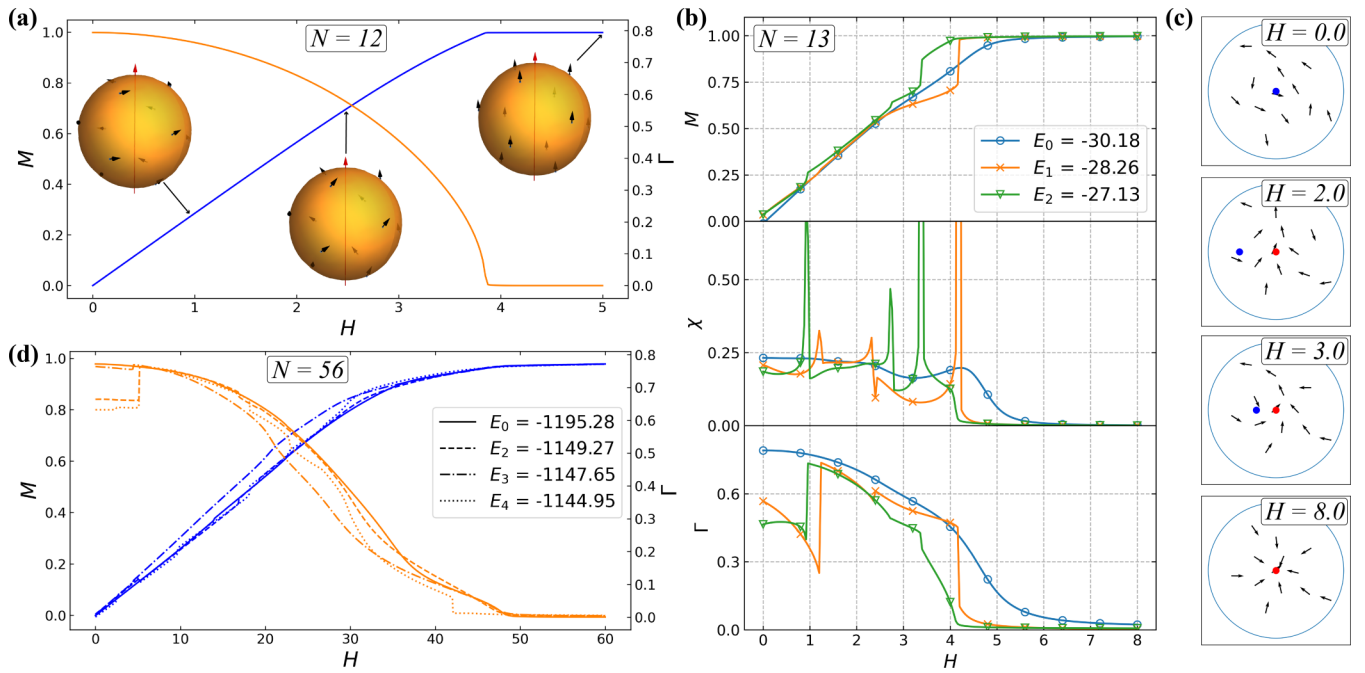
FIG. 4. (a) The magnetization curve (blue, ascending) and magnitude of angular momentum (orange, descending) in dependence on the magnitude of the external field. As shown in complementary 3D visualizations at different values of the external field magnitude ($H = 1.0$, $H = 2.5$, and $H = 5.0$), the dipoles gradually reorient from the initial macrovortex configurations and at high magnitudes fully align with the field. The vertical red arrow shows the direction of the external field. Orientational phase transition in this case is continuous. (b) Magnetization, susceptibility, and magnitude of angular momentum for all three stable configurations of $N = 13$ dipoles. In contrast to the $N = 12$ case, we note multiple discontinuous phase transitions that result in divergences in susceptibility. The jump in Γ at the first phase transition for two excited states shows that, in the external field, some configurations can become more ordered. (c) Azimuthal projection, modified to show normalized projections of dipole orientations to their respective tangent planes, of configurations for the first excited state of $N = 13$ case at different field magnitudes. The blue dot shows the direction of angular momentum Γ for the depicted configuration, and the red dot shows the direction of the external field (aligned with initial Γ of the configuration, always in the center of the diagram). In the first frame, blue and red dots coincide. In the last frame, the direction of Γ is not shown as the magnitude is too small for the quantity to be relevant. (d) Magnetization and Γ magnitude for different configurations of $N = 56$. Discontinuous phase transitions are especially noticeable for the excited states.

the first excited state for $N = 13$, and the fifth excited state for $N = 72$ are shown in Fig. 5. The saturated configuration for $N = 12$ remains metastable for a while when the field is decreasing, which is not the case for $N = 13$ and $N = 72$ states. However, saturation curves for both $N = 56$ and $N = 72$ differ from hysteresis curves, at least, for small magnitudes of the external field which signals that, at saturation, the system loses information on the exact initial dipole orientations. In general, hysteresis is observed for all configurations with no symmetry whereas many symmetric states show no differences between increasing and decreasing fields, e.g., the ground states for $N = 24$ and $N = 72$. Note that dipolar systems on the Fibonacci lattice have a more prominent hysteresis loop with higher remanent magnetization compared to Thomson and Tammes configurations, see the SM [40].

C. Freely rotating sphere

As discussed, the system's response to the external field depends on the field direction. We chose the direction of angular momentum as the characteristic direction of order for each configuration, however, we saw already for the $N = 13$ case that the direction of Γ also changes during the simulations for configurations with no symmetry. This presents the question

of optimal direction of the external field at each magnitude—we seek the direction that minimizes system energy [Eq. (1)] at every step. This is equivalent to the case of a freely rotating sphere which is more relevant for potential experimental realization. We solve this by also minimizing the energy over the field direction. If we write the interaction energy (1) in the form $\mathcal{U}_h = -N\boldsymbol{H} \cdot \boldsymbol{M}$, the optimal external field direction will be parallel to magnetization. With fixed direction of the field, the alignment between field and magnetization was not guaranteed and occurred only at high-field magnitudes.

Figure 6(a) shows susceptibilities and angular momentum magnitudes for the three states of $N = 13$. The excited states undergo an orientational phase transition to join the configuration with that of the ground state. After the initial differences at low fields, the system collapses to the same structure, up to rotations permitted by the symmetry of the positional order. In the saturated configuration, the field is aligned with the symmetry axis of the positional order with the dipole configuration also exhibiting C_{2v} symmetry. Different zero-field configurations can also stay separated until we reach higher external field magnitudes as shown for the case of $N = 56$ in Fig. 6(b). Note that the magnetization and angular momentum magnitude curves for both $N = 13$ and $N = 56$ are different from any of the cases with fixed field direction [Figs. 6(b) and
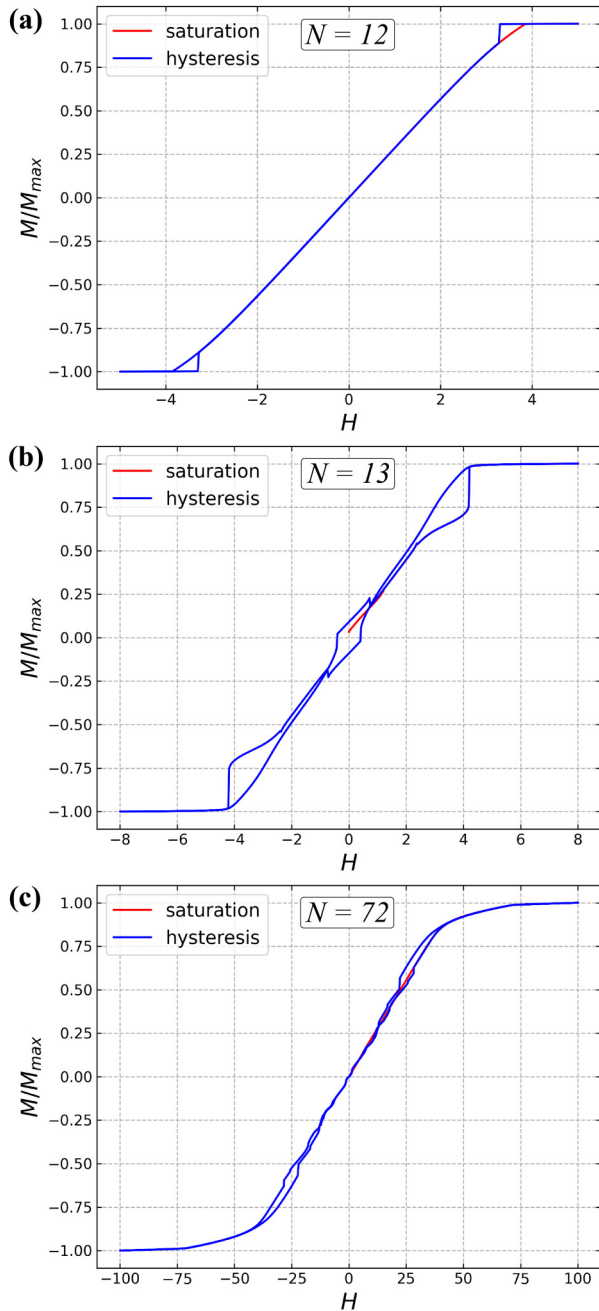
FIG. 5. Hysteresis loops for (a) the ground state for $N = 12$, (b) the first excited state for $N = 13$, and (c) the fifth excited state for $N = 72$. High-symmetry states as well as high-N configurations show weak hysteresis curves while non-symmetric low-N configurations exhibit greater differences between increasing and decreasing field magnetization curves. After saturation, it is possible that the system does not return to the ground state but a state with nonzero remanent magnetization.

FIG. 6. Magnetization and Γ magnitude of a freely rotating sphere in external field for different states of (a) $N = 13$ and (b) $N = 56$. Compared to the results in Fig. 4, the behavior of $N = 13$ states is simplified (the number of phase transitions decreases) whereas the phase transitions for $N = 56$ become more pronounced. In both cases, the configurations at high-field magnitudes are the same for all initial zero-field states. (c) Azimuthal plot for the ground state of $N = 72$ at different external field magnitudes for the case of the freely rotating sphere. The plot is centered to the optimal direction of the external field (red dot), and we can see that the system symmetry changes from C_2 to C_3 and ultimately to C_5. In the last frame, two dipoles on the symmetry axis are not shown as they are oriented perpendicular to the surface and, therefore, have no tangent projection.

6(d)] which means allowing for sphere rotation fundamentally changes dipole states in external field for lattices with no positional symmetry.

For symmetric states where angular momentum is aligned with the rotational symmetry axis, one could expect that the external field remain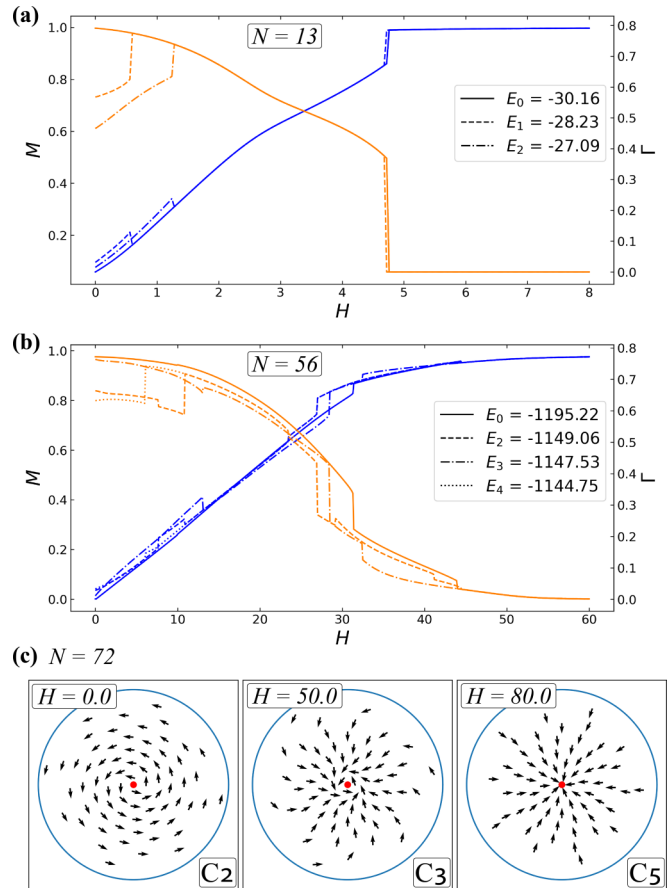s parallel to this axis. This is, indeed, the case for some states, e.g., $N = 12$ where the behavior is exactly the same as for the case with fixed field direction, however, optimal field direction can change for some symmetric states which alongside also changes the configuration symmetry. A notable example is the ground state of $N = 72$. Figure 6(c) shows an azimuthal plot of state configuration at different external field magnitudes. The twofold symmetry of the configuration becomes unstable, and the system transitions to a threefold symmetric state of the first excited state. Finally, at high external field magnitudes, there is another change in optimal field direction where the field aligns with one of the fivefold axes of the positional order. A similar change in symmetry is also observed for the ground state of $N = 24$ that transitions from C_4 symmetry to C_3 at high-field magnitudes.

IV. CONCLUSIONS

We explored orientational ordering of point dipoles on a sphere with positional order fixed in the solutions of the Thomson problem by minimizing the system energy. Some parallels to the 2D Euclidean lattice can be drawn, most notably the universality of the macrovortex ground state that also emerges for the triangular planar lattice. We expect the macrovortex to be the ground state for other spherical lattices that locally resemble a uniform triangular lattice, such as the solutions of the Tammes problem, and the Thomson problem with generalized power laws [3], but for other lattices, such as generalized rhombic lattices (an example being the Fibonacci lattice) or lattices with voids (e.g., the honeycomb lattice), different structures are expected. The macrovortex state is also comparable to the vortex states of the continuous ferromagnetic and spin systems [23,24].

Configuration symmetries as well as the number of different stable states found, depend strongly on the symmetry of the underlying positional order at each N. The symmetry of the dipolar system cannot be higher than the symmetry of the underlying lattice, and in the macrovortex state, can only have a single rotational symmetry axis. We find states belonging to C_2, C_3, and C_4 point groups, however, many macrovortex ground states show no symmetries. In the external field, we discover multiple discontinuous orientational phase transitions, especially for less symmetric states. The direction of angular momentum that characterizes ordering of dipoles can also change as we increase external field magnitude. For the case of a freely rotating sphere where the external field assumes the direction that minimizes system energy, we find that the configurations of different stable states merge with an increasing field. In the saturation configuration, the field is aligned with one of the symmetry axes of positional order.

Studying dipolar interactions of discrete particles on a sphere is a step towards understanding and harnessing the role of anisotropic interactions in stability and structure of spherical assemblies. Many biological structures, such as protomers of viral capsids and RNA nanocages, involve electrostatic interactions in addition to chemical bonds and hard-core repulsion. These interactions are more complex, and are often screened by ions in surrounding medium. Generalizations to more complex anisotropic interactions—screened, quadrupolar, or interactions based on empirical models—are, therefore, important open problems for future investigation. The role of thermal fluctuations can further be explored through Monte Carlo simulations. Another potential research direction is the generalization of the problem to allow for movement of dipoles along the surface of the sphere, which requires addition of a repulsive close-range interaction that prevents aggregation and collapse. This corresponds to possible experimental realizations with interacting colloidal particles. Deviations from a spherical shape and using the anisotropic interactions to drive reshaping of the structures can also be considered. Based on expected stable structures, predicted from simplified models, bottom-up design nanocontainers can be envisioned with self-assembly aided by the anisotropic interactions, and allowing actuation of orientational transitions and changes in symmetry with external fields, giving the potential for controlled rearrangement or dissolution.

[1] J. Thomson, On the structure of the atom: An investigation of the stability and periods of oscillation of a number of corpuscles arranged at equal intervals around the circumference of a circle; with application of the results to the theory of atomic structure, London Edinburgh Dublin Philos. Mag. **7**, 237 (1904).

[2] M. J. Bowick, A. Cacciuto, D. R. Nelson, and A. Travesset, Crystalline particle packings on a sphere with long-range power-law potentials, Phys. Rev. B **73**, 024115 (2006).

[3] E. B. Saff and A. B. J. Kuilaars, Distributing many points on a sphere, Math. Intell. **19**, 5 (1997).

[4] P. Tammes, On the origin of number and arrangement of the places of exit on the surface of pollen-grains, Ph.D. thesis, University of Groningen, 1930.

[5] A. Slosar and R. Podgornik, On the connected-charges Thomson problem, Europhys. Lett. **75**, 631 (2006).

[6] M. Bowick, A. Cacciuto, D. R. Nelson, and A. Travesset, Crystalline Order on a Sphere and the Generalized Thomson Problem, Phys. Rev. Lett. **89**, 185502 (2002).

[7] W. T. M. Irvine, V. Vitelli, and P. M. Chaikin, Pleats in crystals on curved surfaces, Nature (London) **468**, 947 (2010).

[8] D. J. Wales and S. Ulker, Structure and dynamics of spherical crystals characterized for the thomson problem, Phys. Rev. B **74**, 212101 (2006).

[9] D. J. Wales, H. McKay, and E. L. Altschuler, Defect motifs for spherical topologies, Phys. Rev. B **79**, 224115 (2009).

[10] W. L. Miller and A. Cacciuto, Two-dimensional packing of soft particles and the soft generalized Thomson problem, Soft Matter **7**, 7552 (2011).

[11] C. Marzec and L. Day, Pattern formation in icosahedral virus capsids: The papova viruses and nudaurelia capensis beta virus, Biophys. J. **65**, 2559 (1993).

[12] R. Zandi, D. Reguera, R. F. Bruinsma, W. M. Gelbart, and J. Rudnick, From The Cover: Origin of icosahedral symmetry in viruses, Proc. Natl. Acad. Sci. USA **101**, 15556 (2004).

[13] H. W. Kroto, J. R. Heath, S. C. O'Brien, R. F. Curl, and R. E. Smalley, C60: Buckminsterfullerene, Nature (London) **318**, 162 (1985).

[14] Y. Chevalier and M.-A. Bolzinger, Emulsions stabilized with solid nanoparticles: Pickering emulsions, Colloid Surf., A **439**, 23 (2013).

[15] Y. Li, H. Miao, H. Ma, and J. Z. Y. Chen, Topological defects of tetratic liquid-crystal order on a soft spherical surface, Soft Matter **9**, 11461 (2013).

[16] J. D. Luca, S. B. Rodrigues, and Y. Levin, Electromagnetic instability of the Thomson problem, Europhys. Lett. **71**, 84 (2005).

[17] R. Sknepnek and S. Henkes, Active swarms on a sphere, Phys. Rev. E **91**, 022306 (2015).

[18] S. Praetorius, A. Voigt, R. Wittkowski, and H. Löwen, Active crystals on a sphere, Phys. Rev. E **97**, 052615 (2018).

[19] S. Shankar, M. J. Bowick, and M. C. Marchetti, Topological Sound and Flocking on Curved Surfaces, Phys. Rev. X **7**, 031039 (2017).

[20] D. Khoromskaia and G. P. Alexander, Vortex formation and dynamics of defects in active nematic shells, New J. Phys. **19**, 103043 (2017).

[21] P. Renteln, *Manifolds, Tensors, and Forms: An Introduction for Mathematicians and Physicists* (Cambridge University Press, Cambridge, UK, 2014).

[22] A. M. Turner, V. Vitelli, and D. R. Nelson, Vortices on curved surfaces, Rev. Mod. Phys. **82**, 1301 (2010).

[23] M. I. Sloika, D. D. Sheka, V. P. Kravchuk, O. V. Pylypovskyi, and Y. Gaididei, Geometry induced phase transitions in magnetic spherical shell, J. Magn. Magn. Mater. **443**, 404 (2017).

[24] G. Milagre and W. A. Moura-Melo, Magnetic vortex-like excitations on a sphere, Phys. Lett. A **368**, 155 (2007).

[25] M. J. Bowick and L. Giomi, Two-dimensional matter: Order, curvature and defects, Adv. Phys. **58**, 449 (2009).

[26] A. V. Titov and P. Král, Modeling the Self-Assembly of Colloidal Nanorod Superlattices, Nano Lett. **8**, 3605 (2008).

[27] D. V. Talapin, E. V. Shevchenko, C. B. Murray, A. V. Titov, and P. Král, Dipole-dipole Interactions in Nanoparticle Superlattices, Nano Lett. **7**, 1213 (2007).

[28] J. B. Haun, T.-J. Yoon, H. Lee, and R. Weissleder, Magnetic nanoparticle biosensors, WIREs Nanomed. Nanobiotechnol. **2**, 291 (2010).

[29] S. Prakash and C. L. Henley, Ordering due to disorder in dipolar magnets on two-dimensional lattices, Phys. Rev. B **42**, 6574 (1990).

[30] G. O. Zimmerman, A. K. Ibrahim, and F. Y. Wu, Planar classical dipolar system on a honeycomb lattice, Phys. Rev. B **37**, 2059 (1988).

[31] P. I. Belobrov, V. A. Voevodin, and V. A. Ignatchenko, Ground state of a dipole in a plane rhombic lattice, Sov Phys. JETP **61**, 522 (1985).

[32] J. Brankov and D. Danchev, Ground state of an infinite two-dimensional system of dipoles on a lattice with arbitrary rhombicity angle, Physica A **144**, 128 (1987).

[33] L. Abelmann, T. A. G. Hageman, P. A. Löthman, M. Mastrangeli, and M. C. Elwenspoek, Three-dimensional self-assembly using dipolar interaction, Sci. Adv. **6**, eaba2007 (2020).

[34] T. Vissers, Z. Preisler, F. Smallenburg, M. Dijkstra, and F. Sciortino, Predicting crystals of Janus colloids, J. Chem. Phys. **138**, 164505 (2013).

[35] E. Y. Vedmedenko, A. Ghazali, and J.-C. S. Lévy, Magnetic vortices in ultrathin films, Phys. Rev. B **59**, 3329 (1999).

[36] E. Y. Vedmedenko, N. Mikuszeit, H. P. Oepen, and R. Wiesendanger, Multipolar Ordering and Magnetization Reversal in Two-Dimensional Nanomagnet Arrays, Phys. Rev. Lett. **95**, 207202 (2005).

[37] E. Vedmedenko, S. E.-D. Mandel, and R. Lifshitz, In search of multipolar order on the penrose tiling, Philos. Mag. **88**, 2197 (2008).

[38] A. Baskin, W.-Y. Lo, and P. Král, Clusters and Lattices of Particles Stabilized by Dipolar Coupling, ACS Nano **6**, 6083 (2012).

[39] R. G. Barrera, G. A. Estevez, and J. Giraldo, Vector spherical harmonics and their application to magnetostatics, Eur. J. Phys. **6**, 287 (1985).

[40] See Supplemental Material at http://link.aps.org/supplemental/10.1103/PhysRevB.102.075416 for details on dipolar states on Tammes and Fibonacci lattices.